Article

Using Structure Location Data to Map the Wildland–Urban Interface in Montana, USA

Alexander R. Ketchpaw [1], Dapeng Li [1,*], Shahid Nawaz Khan [1,2], Yuhan Jiang [3], Yingru Li [4] and Ling Zhang [5]

1 Geospatial Sciences Center of Excellence, Department of Geography and Geospatial Sciences, South Dakota State University, Wecota Hall 115, Box 506, 1101 Medary Ave., Brookings, SD 57007, USA
2 Institute of Geographical Information Systems, National University of Sciences and Technology, Islamabad 44000, Pakistan
3 Department of Built Environment, North Carolina A&T State University, Greensboro, NC 27411, USA
4 Department of Sociology, University of Central Florida, 4297 Andromeda Loop N., Howard Phillips Hall, Room 403, Orlando, FL 32816, USA
5 Department of Geography, University of Central Arkansas, 318 Burdick Hall, 201 Donaghey Avenue, Conway, AR 72035, USA
* Correspondence: dapeng.li@sdstate.edu; Tel.: +1-605-688-4620

Abstract: The increasing wildfire activity and rapid population growth in the wildland–urban interface (WUI) have made more Americans exposed to wildfire risk. WUI mapping plays a significant role in wildfire management. This study used the Microsoft building footprint (MBF) and the Montana address/structure framework datasets to map the WUI in Montana. A systematic comparison of the following three types of WUI was performed: the WUI maps derived from the Montana address/structure framework dataset (WUI-P), the WUI maps derived from the MBF dataset (WUI-S), and the Radeloff WUI map derived from census data (WUI-Z). The results show that WUI-S and WUI-P are greater than WUI-Z in the WUI area. Moreover, WUI-S has more WUI area than WUI-P due to the inclusion of all structures rather than just address points. Spatial analysis revealed clusters of high percentage WUI area in western Montana and low percentage WUI area in eastern Montana, which is likely related to a combination of factors including topography and population density. A web GIS application was also developed to facilitate the dissemination of the resulting WUI maps and allow visual comparison between the three WUI types. This study demonstrated that the MBF can be a useful resource for mapping the WUI and could be used in place of a national address point dataset.

Keywords: wildland–urban interface; structure point data; address point data; web GIS

1. Introduction

The past few years have witnessed the rapid increase of the total wildland–urban interface (WUI) area [1,2] and the number of homes located within the WUI in the U.S. [1,3]. Additionally, there has been a rise in wildfire suppression and mitigation costs [3]. The WUI grew from 7.2% of the total land area in 1990 to 9.5% in 2010, adding 189,000 km^2 of land classified as WUI and 12.7 million housing units in the WUI in the U.S. [1]. According to a recent study, the number of residential homes within the WUI in the U.S. has reached 49 million [3]. Theobald and Romme [2] have also projected that the WUI in the U.S. will grow by more than 10% by 2030 as more people move to rural and suburban communities. The WUI is defined as the area where a built environment meets the wildland [4]. In the Federal Register, Glickman and Babbitt [4] define the WUI as a populated area in which structures are adjacent to or intermingle with wildland vegetation. There are three main WUI categories: interface, intermix, and occluded WUI [4]. Interface WUI is where structures and wildland vegetation touch, separated by a clearly defined boundary [4].

An expanded version of this definition states that interface WUI is where housing units are within 2.4 km of a 5 km^2 or larger patch of vegetation with more than 75% wildland cover [1,5]. The structures in an intermix WUI occur within unbroken wildland vegetation but must have a minimum housing density of one house per 40 acres (6.17 houses per km^2) [4]. This definition has been refined to state that wildland vegetation must cover at least 50% of the area where the structures occur in an intermix WUI area [1,5]. Occluded WUI exists where there is an area of wildland fuels surrounded by urban structures (e.g., the green spaces within an urban area) [4]. Of these three types of WUI, interface and intermix WUI have been widely used in WUI mapping research [1,5–7]. The WUI definition in the Federal Register focuses specifically on housing units as defined in the U.S. Census housing density data when determining structure density [1,5]. While there is extensive use of the Federal Register WUI definition in WUI mapping, some researchers use other factors to define the WUI. For example, researchers in Canada expanded the WUI definition to include two other WUI types: WUI-Ind (industrial) and WUI-Inf (infrastructural) [8]. The inclusion of industrial buildings and other structures when defining the WUI may be necessary due to the possible impacts of wildfire on these assets during and after incidents [8]. Similarly, the inclusion of infrastructure in the WUI definition may also be important as these structures are related to evacuation and fire protection [8]. Infrastructure networks (e.g., roads, railroads, and powerlines) could also be sources of wildfire ignition [8–10]. Using industrial and infrastructural assets to determine where the WUI is located expands the area significantly, mainly where infrastructure-related structures are present [8].

Over the past several decades, there has been an increasing trend of significant wildfire occurrence in the western U.S. [11,12] as well as an increase in the area burned by wildfire annually [1,3,12]. As climate change has progressed in recent years, there has been a decrease in precipitation during fire seasons [12] along with an increase in wildland fuel dryness [13]. As fuel dryness increases, wildfire risk [14] and the total area burned will likely increase as well [3,12]. Wildfire risk can be defined as the combination of three factors: the probability of ignition, the intensity of the fire, and the impacts of the fire on the landscape [15]. One aspect of wildfire risk is the loss of lives and casualties in wildfires. Between 2014 and 2018, 57 wildfires resulted in casualties, the worst being the Camp Fire in Paradise, California in 2018 with 85 fatalities [16]. Due to drier fuels [12,13], high incidence of anthropogenic wildfire ignition [17], and the expanding WUI, the wildfire risk in the WUI is likely to increase [1]. Another aspect of wildfire risk within WUI communities is structure loss. Multiple recent studies examined the factors that determine the likelihood of structure loss within WUI communities [18–20]. For example, in a study conducted by Syphard et al. [21], the main focus is on how the spatial grouping of structures and other factors such as slope, aspect, and elevation relate to structure loss in wildfires. Other research considers different factors such as building materials and construction, risk mitigation practices such as defensible space, and regional variation that may impact structure loss [20]. As the WUI expands, significantly more structures are at risk of damage or destruction by wildfire [1,22]. The increasing risk of structure loss related to wildfire within the WUI tends to drive research as well [20,21,23–25]. Understanding where the WUI exists is essential when combined with wildfire risk data to formulate decisions related to the management and mitigation of wildfire [26]. A better understanding of wildfire risk can facilitate decision-making in wildfire policy, fuel management, and community planning in the WUI [27]. The analysis of wildfire risk is crucial in wildfire management with more frequent, destructive wildfires occurring in the American west [11,19]. For example, wildfire risk information can be used to establish defensible space regulations to reduce structure loss in wildfires and distribute wildfire management resources.

Wildfire management (e.g., wildfire prevention, suppression, and mitigation) has become more challenging as the WUI expands [1], anthropogenic wildfires in the U.S. become predominant [9,17], and wildfires in the WUI are expected to increase [24]. As a result, WUI mapping becomes crucial for decision-making in wildfire management. In the early 2000s, WUI research received attention as wildfire and structure loss increased significantly [6].

However, even with increased attention to the WUI problem, a national WUI map did not exist [6]. This led to the development of a national WUI dataset based on census block data and the United States Geological Survey (USGS) National Land Cover Database (NLCD) [6]. Since then, many studies have been conducted to develop or refine different methods to map the WUI within the U.S. [2,5,6,28,29] and internationally [8,30–33]. Note that different types of data can be used in different WUI mapping methods. For example, Radeloff et al. [6] produced their WUI map at a national scale using the structure density in each census block derived from the US Census housing unit counts and vegetative cover data from the USGS NLCD. One limitation of the census-block-based methods is related to the distribution of structures within a census block. For example, many structures could be concentrated in a small area within a large census block so that the structure density meets the criteria for inclusion in the WUI classification. This allows for the entire census block to be classified as WUI even though a large portion of the area does not meet the WUI criteria. This could lead to less precise WUI and possible bias due to the uneven spatial distribution of structures within a census block [28,34]. Another limitation is the decreased applicability to local and regional scales when it is crucial to understand where structures are located during and before a wildfire [28,34].

Another popular way to map the WUI is to use the fine-grained structure location data instead of the housing unit count data from the U.S. Census [23,28,29]. Using exact structure locations to map the WUI allows for a higher level of precision [8,28,29]. For example, Johnston and Flannigan [8] utilized physical structure locations from an open structure database named CanVec+ in Canada to map the WUI. Additionally, Bar-Massada et al. [28] used the structure locations derived from government agency data and digitized from satellite and aerial imagery to map the WUI. Moreover, we can also compile structure location data from other sources such as parcel centroids [29] or address point data [35]. Address point data only includes structures with known addresses, excluding some structures from the mapping process [35]. In the U.S., the Department of Transportation is working with local and state governments to aggregate state, local, and tribal datasets into one cohesive national address point database [35]. However, a complete national address point dataset is not currently available because some states have address point datasets that exist but are not completely within the public domain [35]. Thus, it is difficult to use address point data to produce a national WUI map. A relatively recently developed dataset that may be useful as an alternative to address point data is the Microsoft Building Footprint (MBF) dataset [36]. This polygon dataset includes all the structure footprints derived from a machine learning algorithm in the U.S. [36]. The MBF dataset presents an opportunity to derive more accurate WUI maps based on structure locations. The MBF dataset has been used in population distribution mapping [37], wildfire-related structure loss [23], flood exposure [38], and WUI mapping [39–41]. The release of the MBF dataset makes it possible to produce a structure-based WUI map for the whole U.S. The type of structure location dataset (address point or physical structure location) could also produce variations in the WUI map. Although different types of structure location data exist and can be used for WUI mapping, little research has been done to compare these datasets in WUI mapping. Since address point data and the MBF dataset are two popular datasets used in WUI mapping, we chose to examine the differences of these two types of structure location data in WUI mapping in this study.

This study focused on using two different structure location datasets to improve WUI mapping in Montana. The research objectives of this study were to: (1) derive WUI maps using the MBF and the Montana structure point datasets; (2) compare the following three types of WUI maps in Montana: the WUI maps derived from the Montana structure point dataset (WUI-P), the WUI maps derived from the MBF dataset (WUI-S), and the Radeloff WUI map derived from census data (WUI-Z); (3) analyze the spatial patterns of the derived WUI-P and WUI-S at the county level; and (4) develop a web geographic information system (GIS) application to map the three types of WUI. The novelty of this study is as follows. First, two different structure location datasets were used to map the WUI in

Montana. Second, a systematic comparison of the three types of WUI maps in Montana is provided. The remainder of this article is organized as follows. Section 2 details the study area and the data employed in the study. The proposed methods are included in Section 3. The results are presented in Section 4. The discussion and conclusion are in Sections 5 and 6, respectively.

2. Study Area

The study area is the state of Montana (Figure 1). Montana is in the northwest portion of the U.S. The Continental Divide splits Montana into two distinct climate regions, with a maritime-like climate where cooler summer months with mild winters are common to the west of the divide and hotter summers and colder winters associated with a semi-arid continental climate to the east of the divide [42]. Precipitation in these two regions also differs significantly. The western part of the state experiences higher precipitation with an average of 56–76 cm annually predominantly occurring in winter and spring [43]. In the eastern plains, the semi-arid climate provides less precipitation with an average of 30–36 cm annually [43]. The total area of the state is 380,831 km^2 [44], and it had an estimated population of 1,068,778 as of 1 July 2019 [45]. Within Montana, the population in 2010 was more concentrated in the western portion of the state where counties with the largest population included Flathead, Missoula, Cascade, Lewis and Clark, and Gallatin. Montana was chosen as the study area due to the rapid WUI expansion in the state, the high percentage of residents in the WUI, and the availability of a statewide structure/address point dataset from the Montana State Library. In Montana, the total area classified as WUI in 2010 was 5304 km^2, which was only 1.4% of the total area (an increase of 67% between 1990 and 2010) of the state but contained 62.3% of the state's population and 63.9% of the housing units in Montana [44].

The two main types of data required for WUI mapping are vegetation cover data and structure location data [28]. Table 1 presents the details on each of the datasets used in this study. To ensure accurate analysis, all datasets were projected to the North American Datum (NAD) 1983 2011 State Plane Montana coordinate system to match the address point data obtained from the Montana State Library Geographic Information Services.

Table 1. The datasets used in this study.

| Data	Data Source	Date	Format
Microsoft building footprint data	Microsoft	2018	Vector (polygon)
Montana structure/address framework	Montana State Library Geographic Information Services	2020	Vector (point)
Vegetation cover data (NLCD)	U.S. Geological Survey	2016	Raster
Montana state boundary	Montana State Library Geographic Information Services	2020	Vector (polygon)
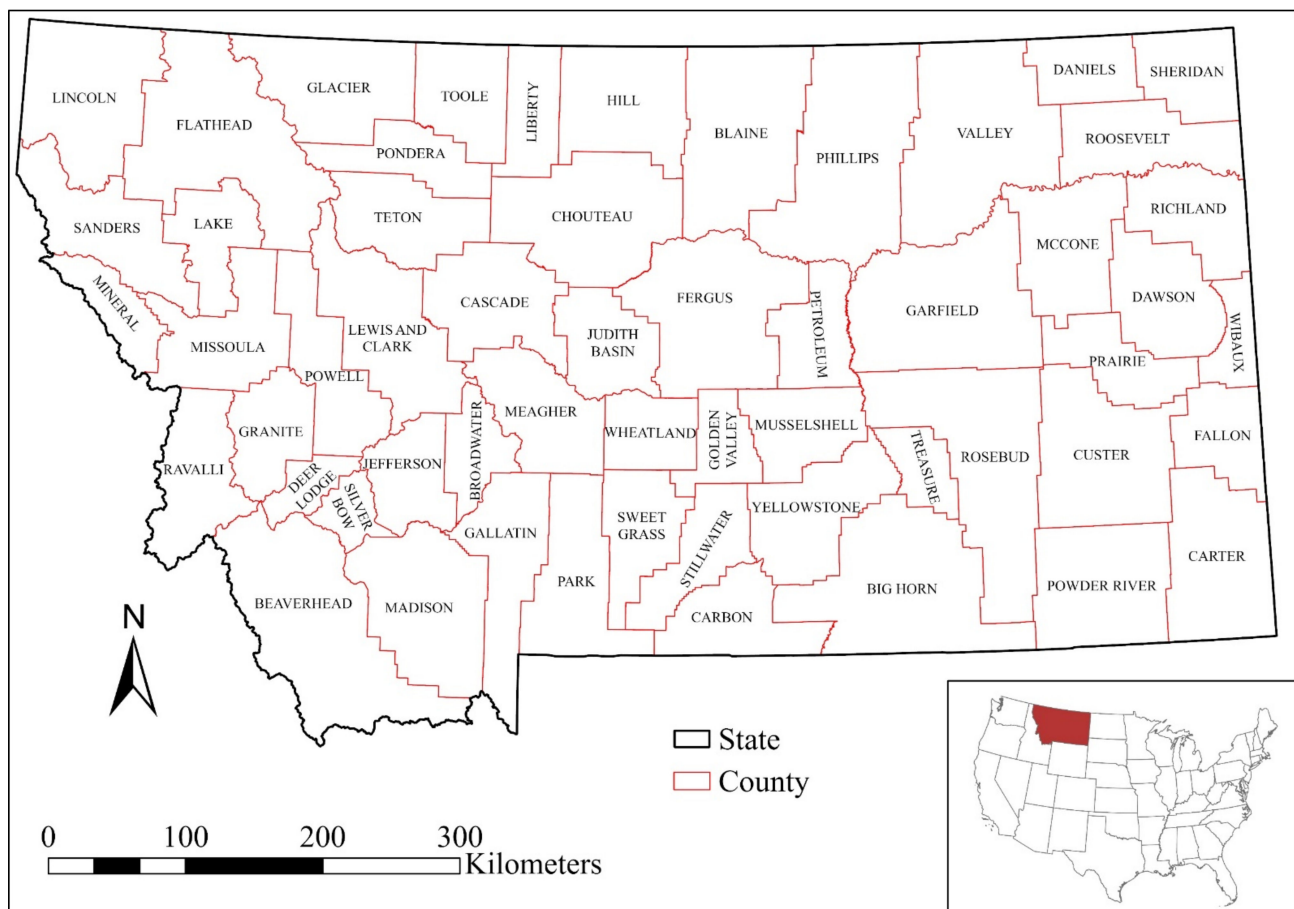
Figure 1. The map of the study area.

3. Methods

3.1. Mapping the WUI

The flowchart in Figure 2 outlines the key steps for mapping WUI-P and WUI-S. We used the WUI mapping method proposed by Bar-Massada et al. [28] to map the WUI in Montana. This method requires two input datasets: structure location data and vegetation cover data [28]. We used Python and the ArcPy library of ArcGIS Pro 2.9 to generate WUI-P and WUI-S maps. The Python script was executed for two structure location datasets with different buffer distances. Initially, we used a buffer polygon of the state boundary to extract the vegetation cover data from NLCD to ensure there was no edge bias near the Montana state border. We used the data management tools (feature to point function) in ArcGIS Pro 2.9 to extract the centroids of the building footprint polygons from the MBF and derived a point dataset. Then we employed the two structure location datasets to derive the structure/housing density for the study area. The calculation was accomplished by using a buffer for each pixel in the 30 m NLCD raster. Note that the area and shape of the WUI will vary with buffer distance and the WUI generated with different buffer distances can be used for different purposes [28]. Based on the parameters used by Bar-Massada et al. in a previous study [28], we chose to use buffer distances ranging from 100 m to 1000 m with a 100 m interval so that we could compare the WUI generated with two different structure location datasets at different buffer distances. This calculation produces the structure density per km^2 at each buffer distance. Then we reclassified the structure density raster based on the following rule: '1' was assigned to the pixels where the structure density was larger than 6.17 structures/km^2, and '0' was assigned to the pixels with a structure density equal to or smaller than 6.17 structures/km^2. This new raster was then compared to the vegetation cover dataset to determine each pixel's WUI classification. Specifically,

any pixel with a structure density of larger than 6.17 structures/km^2 and a vegetation cover larger than 50% in the buffer was classified as intermix WUI; a pixel was classified as interface WUI if the pixel had a structure density above 6.17 structures/km^2 and a vegetation cover equal to or smaller than 50% but was within 2.4 km of a 5 km^2 or larger patch of continuous vegetation. After the WUI maps were generated, we used the ArcGIS Pro Calculate Geometry tool to calculate the area of the WUI and employed the ArcGIS Pro Aggregate Points tool to derive the number of structures that fell within the WUI.
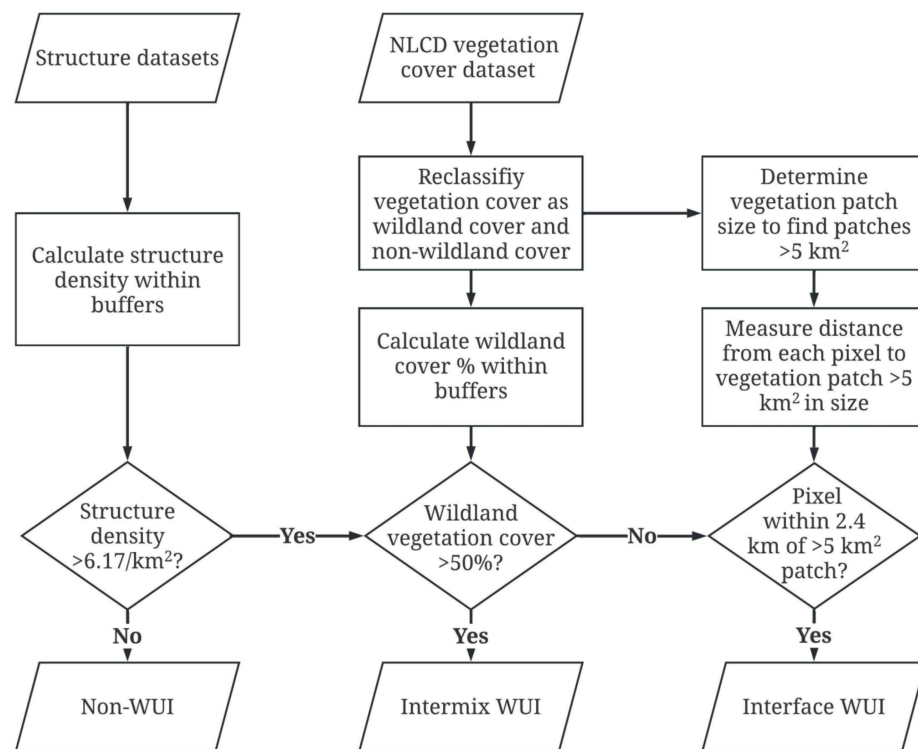

Figure 2. The flowchart of the WUI mapping procedure.

3.2. Map Comparison

We used GIS to compare WUI-P, WUI-S, and WUI-Z. Specifically, the WUI-Z is used as the validation dataset to derive the confusion matrices [28]. This comparison method will show how much area each WUI dataset shares and how much area each dataset identified as WUI or non-WUI as compared to the other. The comparison results can provide insight into which WUI dataset is more similar to the WUI-Z map. The comparison of the two datasets will demonstrate how the inclusion of all structures influences the total area and spatial patterns of the WUI. Figure 3 shows the detailed comparison procedure. We used the intersect function in ArcGIS Pro to calculate the overlap between the WUI-P, WUI-S, and WUI-Z layers to accomplish the spatial comparison. The results were aggregated into a matrix detailing the total area of each WUI map shares with another, the total area that was classified as WUI in one map but not the other, and the total area that both WUI maps classified as non-WUI. To ensure that only the areas classified as WUI were considered, all areas classified as non-WUI were ignored when calculating the percentage agreement. The map comparison process determined the agreement between WUI-P, WUI-S, and WUI-Z.
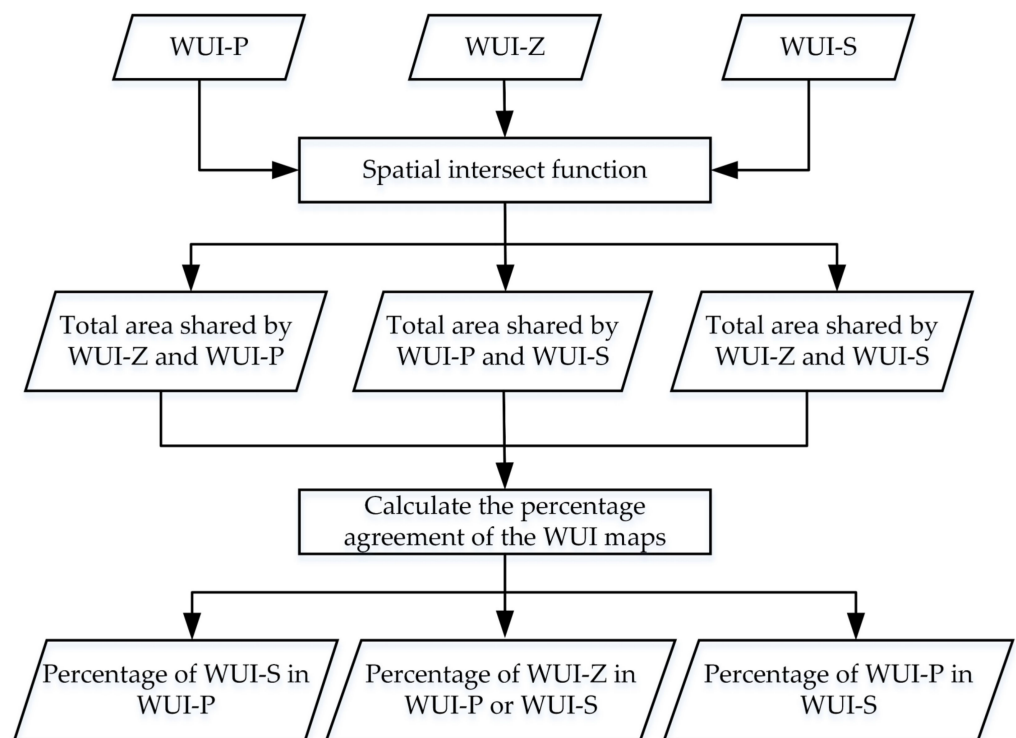
Figure 3. The flowchart of the WUI mapping procedure.

3.3. Estimating WUI Population

Another factor that could be compared between WUI-P and WUI-S is the percentage of the population that resides within the WUI. It is straightforward to calculate the population in WUI-Z due to the direct use of census blocks in the method [6]. However, it was more complicated to determine the population within the WUI-P or WUI-S. The shapes of WUI-P and WUI-S were irregular, which made it difficult to leverage census data to calculate WUI population. As a result, we used dasymetric mapping to address this issue. Dasymetric mapping involves the use of secondary data to refine primary data to be used in further analysis, including estimation of population distribution [46,47]. We used the method proposed by Tapp [46] to calculate the population per address point or structure location within a census block group. While the use of census block level population could provide a more precise population estimate, the use of block group population was adopted in this case. This is because many census blocks that are populated do not contain any structure points from either structure location dataset. With the population per point calculated, we employed the "summarize within" function in ArcGIS Pro to derive the total population falling within the WUI. We used Python and ArcPy to automate the calculation process to generate the results for each WUI polygon to increase efficiency.

3.4. Spatial Analysis of WUI

We employed the global and local Moran's I [48] to study the spatial patterns of the derived WUI-P and WUI-S at the county level in Montana. Specifically, this analysis focused on two variables: the percentage area of the county defined as WUI (p_a) and the percentage of structures or address points within the WUI for each county (p_s). The null hypothesis was that the WUI is randomly dispersed at the county level. The results were compared to various geographical aspects of Montana to explain the spatial patterns. The results of spatial analysis can be utilized by community planners and wildfire managers. For example, the county-level spatial cluster information can provide insight into where resources can be most effective in community planning or wildfire management. Moreover,

the results could also be used by county governments to develop their community wildfire protection plan (CWPP).

First, we used the global Moran's I to determine if spatial autocorrelation existed at the county level in Montana. This calculation produces a value, I, that falls between -1 and 1. A value of -1 represents an instance where no neighbors share the same value (perfect negative autocorrelation), while a value of 0 is an instance where little to no spatial autocorrelation has occurred (random occurrence of values), and a value of 1 indicates perfect autocorrelation (similar values are clustered together) [48]. A z-score and a *p*-value are also derived in global Moran's I analysis. The *p*-value is used to determine whether the null hypothesis can be rejected. Once the global Moran's I is derived, the next step is to use the local Moran's I [48] to identify the locations of clusters. When applied to a dataset, each observation is calculated separately to generate a local Moran's I statistic. In the case of this study, each county within Montana represented an observation of the two variables being tested. Once the local Moran's I for an observation was determined, a z-score was calculated. The z-score was used to determine if an observation was surrounded by neighbors that had similar values or not. If the z-score for an observation has a high positive value, it is likely to be surrounded by neighbors with similar values; and if the observation has a large negative z-score, it is likely to be surrounded by dissimilar neighbors [49]. The values of an observation and its neighbors can be defined as having a high–high (HH), low–low (LL), low–high (LH), or high–low (HL) relationships [50]. Both HH and LL will have positive local Moran's I values, while LH and HL will have negative local Moran's I values [50]. To determine if the generated values are statistically significant, a pseudo *p*-value is calculated [48]. We used Python and ArcPy to perform the spatial analysis. The outputs are individual feature classes for local Moran's I and an HTML report for global Moran's I for each buffer distance, structure location dataset, and variable.

3.5. Web Mapping

A web GIS application (https://tinyurl.com/2p8rajju, accessed on 16 July 2022) was developed to disseminate the results of this study. The web GIS application includes three types of WUI maps: WUI-P, WUI-S, and WUI-Z. The users of the web GIS application may include, but are not limited to researchers, stakeholders, and the public. Specifically, researchers can use the web GIS application to compare the WUI maps derived from different methods and data; stakeholders can employ the web GIS application to check different WUI maps to facilitate their decision-making; and the public can access the WUI maps via the web GIS application to evaluate possible wildfire risk in a specific area. The web GIS application includes the search tool that allows the users to zoom in to a specific location to check the WUI maps. The system architecture of the web GIS is shown in Figure 4. Within this system most of the computation is handled on the server side (i.e., the web server or the GIS server). The user can use a web browser (client) to access the web GIS. To ensure the results are available to anyone who may need it, the web GIS application will not require users to log into the system to access the data. By presenting the data in a web GIS in this manner, the data will be accessible to anyone who could use it to supplement any decisions that they may need to make related to wildfire.
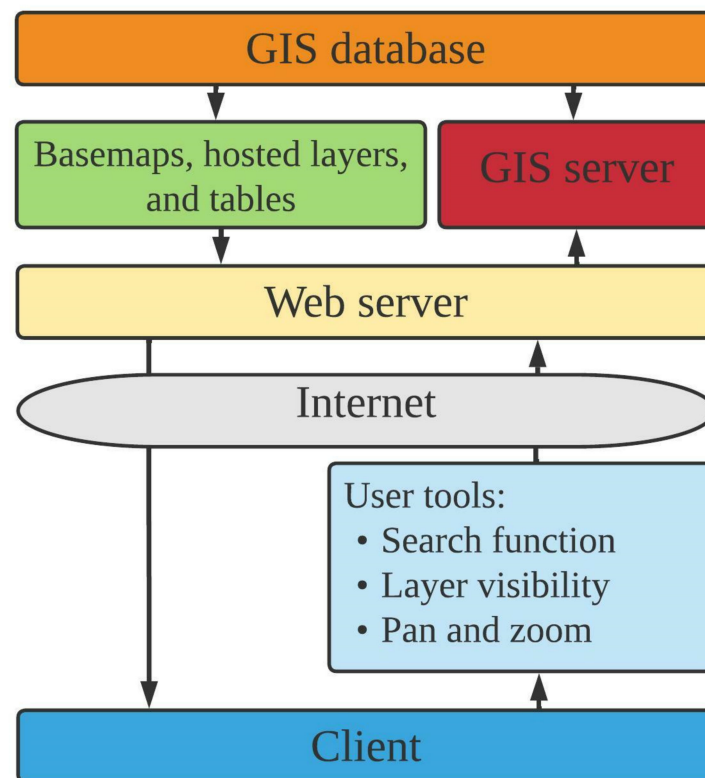
Figure 4. The system architecture of the web GIS.

The design of the graphical user interface (GUI) of the web GIS application is shown in Figure 5. This design was chosen to ensure that the data presented could be easily interpreted and accessed. To allow users to perform direct comparisons, these WUI maps are arranged as three separate map windows placed in a row. We used a dashboard style web application in ArcGIS Online [51] to make sure that each of the three maps could be presented to allow easy comparison. This style of web GIS also allows more data to be easily accessed, through the inclusion of graphs, charts, or tables as well as descriptive text which can also provide links to external sources. Our web GIS application also has a search tool, which allows the user to locate points of interest and determine how the theme of the web GIS applies at that location.

We used ArcGIS Online to implement the web GIS application. When setting up a web GIS, it is important to consider how to optimize the system. Due to the large size of the WUI maps, we used map tiling to improve system performance. Map tiling is a practice where a series of tiles are generated to represent the feature that will be displayed and then cached on the web server, which improves client-side performance as well as usability and scalability [52]. The specific type of map tile used for this web GIS was vector tiles as opposed to raster tiles. We used ArcGIS Pro to generate the tiles and upload them to ArcGIS Online. While vector tiles can improve the performance of a web GIS, they also have some limitations. For instance, unlike a non-tiled vector feature class layer, a vector tile layer has limited interactability. Vector tiles in ArcGIS Online do not currently have the option to enable pop-up boxes when clicked. This limitation is not of concern for this study because the web GIS is only meant to be used as a visual comparison tool for different WUI maps. Another limitation is that we cannot directly add a legend for a vector tile layer in ArcGIS Online. In order to overcome this limitation, the WUI-Z layer was not converted to a vector tile layer and the legend was based on this layer. Thus, the symbology of the WUI-S and WUI-P layers was set to match that of the WUI-Z layer.
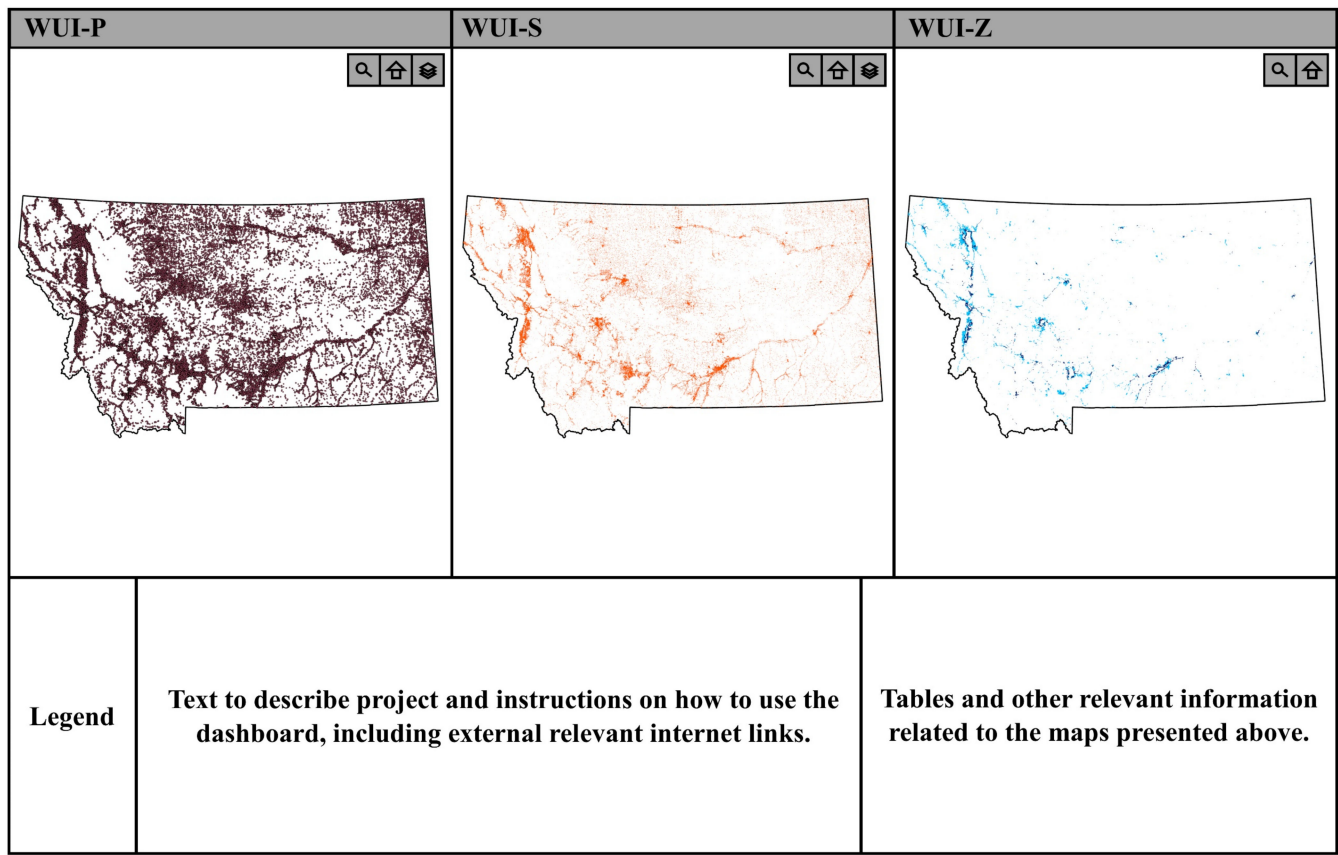
Figure 5. The design of the graphical user interface (GUI) for the web GIS application.

4. Results

4.1. WUI Maps

The results include ten WUI-P layers and ten WUI-S layers. Each of the ten maps represents one of the WUI maps generated with a buffer distance ranging from 100 m to 1000 m (with a 100 m interval). The total areas of interface and intermix WUI for WUI-P and WUI-S are shown in Table 2. The results show that the area of intermix WUI is greater than that of the interface WUI at all buffer distances in both WUI-P and WUI-S. For each structure location dataset, the WUI area initially starts small, increases, and then decreases as the buffer distance increases. At the 100 m buffer distance, the total WUI for both WUI-P and WUI-S is below 10,000 km^2, and the difference is within 2000 km^2. However, as the buffer distance increases, the gap in area widens with WUI-S consistently being more than 3000 km^2 greater in area, peaking at nearly 10,000 km^2 more than WUI-P at 500 m and 600 m buffer distances. The total WUI in WUI-P peaks at 12,073.90 km^2 at 200 m buffer distance. The largest area for WUI-S is 19,878.45 km^2 at a buffer distance of 500 m. The larger area defined as WUI in WUI-S is most likely due to the greater number of structures included as opposed to single addresses, especially in rural areas.

Table 2. The area of different types of WUI in WUI-P and WUI-S (unit: km²).

Buffer Distance (m)	Intermix WUI-P	Interface WUI-P	WUI-P	Intermix WUI-S	Interface WUI-S	WUI-S
100	3403.18	1552.80	4955.98	4201.29	1981.58	6182.88
200	8686.18	3387.73	12,073.90	10,590.12	4434.30	15,024.43
300	7777.51	3172.98	10,950.48	11,904.26	5448.97	17,353.23
400	6139.58	2508.00	8647.58	11,151.68	5584.64	16,736.32
500	7139.12	2768.52	9907.64	13,259.49	6618.96	19,878.45
600	7193.79	2750.59	9944.38	13,031.34	6603.06	19,634.40
700	6923.42	2655.90	9579.32	11,429.46	5842.45	17,271.91
800	7018.06	2658.73	9676.79	10,751.28	5365.80	16,117.08
900	7286.63	2728.69	10,015.32	10,526.75	5191.54	15,718.29
1000	7338.08	2745.20	10,083.28	10,090.48	4854.59	14,945.07

Another important aspect to examine is how many structures fall within the WUI. The overall total number of structures within the WUI-S is the highest at the 100 m buffer and decreases as the buffer distances increase (Table 3). The intermix WUI in WUI-S contains more structures than that in WUI-P at each buffer distance. The number of structures within intermix WUI-P at each buffer distance behaves somewhat differently than interface WUI-P and both intermix and interface WUI-S. The main difference is while the total number of structures starts off high (193,250 structures within intermix WUI-P at 100 m), the number of WUI-P intermix structures decreases to a minimum of 164,343 structures at 400 m, which then increases to 178,112 WUI-P intermix structures at 1000 m with some slight fluctuation as the buffer distance increases.

Table 3. The number of structures within WUI-P and WUI-S.

Buffer Distance (m)	Intermix WUI-P	Interface WUI-P	WUI-P	Intermix WUI-S	Interface WUI-S	WUI-S
100	193,205	333,031	526,236	293,055	348,807	641,862
200	194,536	330,912	525,448	286,643	353,281	639,924
300	178,304	320,778	499,082	270,657	348,779	619,436
400	164,343	309,183	473,526	251,476	338,938	590,414
500	169,876	302,770	472,646	250,686	332,990	583,676
600	169,342	297,328	466,670	239,243	323,569	562,812
700	168,044	291,569	459,613	222,348	310,722	533,070
800	172,147	283,491	455,638	215,752	298,227	513,979
900	175,652	278,220	453,872	212,330	290,240	502,570
1000	178,112	272,701	450,813	209,434	281,788	491,222

While the total number of structures within the intermix WUI differ greatly between WUI-P and WUI-S, the difference in the total number of structures within the interface WUI is much smaller. With the difference within the intermix WUI ranging between about 31,000 at 1000 m to approximately 100,000 at 100 m, the difference between the total number of structures within interface WUI-P and WUI-S ranges from just over 9000 at 1000 m to a maximum of approximately 30,000 at 500 m.

4.2. Map Comparison

The map comparison procedure generated multiple vector datasets representing the total area that each WUI shared with other types of WUI. Figure 6 shows how each WUI relates to other types of WUI at 100 m, 500 m, and 1000 m buffer distances around Billings, Montana. The differences between WUI-P and WUI-S are minor, with WUI-S appearing to cover more area. This difference is likely due to the inclusion of all structures instead of just address points. WUI-P and WUI-S have a larger area of WUI than WUI-Z at each buffer distance except WUI-P at 100 m. This difference is likely due to two factors: the use

of precise structure location in WUI-P and WUI-S and the use of only housing units when calculating structure density in each census block in WUI-Z (the WUI-P and WUI-S use all structure points regardless of their classification). Table A1 includes the area shared between WUI-P and WUI-S at each buffer distance and along with the area each WUI shares with WUI-Z. WUI-P and WUI-S may show a more precise WUI location due to exact the structure points used to define WUI classification rather than the blanket housing density used to determine WUI-Z classification. Dividing the area shared between WUI-P, WUI-S, and WUI-Z (Table A1) by the combined area classified as WUI in each pairing produces the percentage agreement between each WUI. Table A2 includes the percentage of WUI-S that agrees with both WUI-P and WUI-Z at each buffer distance. Figure 7 illustrates the percentage agreement at each buffer distance. The percentage agreement between WUI-P and WUI-S varies between 42.60% and 58.57%. The low percentage agreement values occur at buffer distances of 400 m, 500 m, and 600 m, and the high percentage agreement values occur at 200 m and 1000 m. While the percentage agreement between WUI-P and WUI-S did not drop below 40.00%, the percentage agreement between WUI-P and WUI-Z was always below 40.00% and the agreement between WUI-S and WUI-Z was never above 30.00%.

4.3. WUI Population Estimates

Performing basic dasymetric population mapping showed that differences between each buffer level and point dataset were relatively minor (Table 4). Table 4 contains the results showing the estimated populations in the WUI-P and WUI-S at each buffer level and WUI-Z within non-WUI, interface WUI, and intermix WUI. In all cases, the point-based WUI methods encapsulate more of the population within intermix and interface WUI. However, as the buffer distance increases, the percentage of the total population within the WUI decreases. Figure 8 illustrates the downward trend of the percentage of population within the WUI-P and WUI-S at each buffer distance as well as the comparison to the percentage population within WUI-Z.

Table 4. The estimated population within the WUI.

| WUI Type	Buffer Distance (m)	Non-WUI Population (2010)	Intermix-WUI Population (2010)	Interface-WUI Population (2010)	Total Population (2010)	Percentage Population in WUI (2010)
WUI-Z	NA	373,358	155,175	460,882	989,415	62.26%
WUI-P	100	224,904	231,378	533,133	989,415	77.27%
	200	226,189	232,753	530,472	989,415	77.14%
	300	259,835	213,634	515,946	989,415	73.74%
	400	289,931	198,440	501,044	989,415	70.70%
	500	289,560	206,089	493,766	989,415	70.73%
	600	297,209	206,534	485,672	989,415	69.96%
	700	305,439	205,615	478,361	989,415	69.13%
	800	309,969	211,182	468,265	989,415	68.67%
	900	311,752	216,063	461,600	989,415	68.49%
	1000	315,182	219,568	454,665	989,415	68.14%
WUI-S	100	222,570	247,920	518,925	989,415	77.50%
	200	224,085	245,385	519,945	989,415	77.35%
	300	237,006	237,926	514,483	989,415	76.05%
	400	255,618	227,877	505,920	989,415	74.16%
	500	258,819	231,159	499,437	989,415	73.84%
	600	270,419	227,018	491,978	989,415	72.67%
	700	287,015	219,728	482,672	989,415	70.99%
	800	297,194	220,363	471,858	989,415	69.96%
	900	303,113	222,037	464,265	989,415	69.36%
	1000	310,007	223,002	456,406	989,415	68.67%
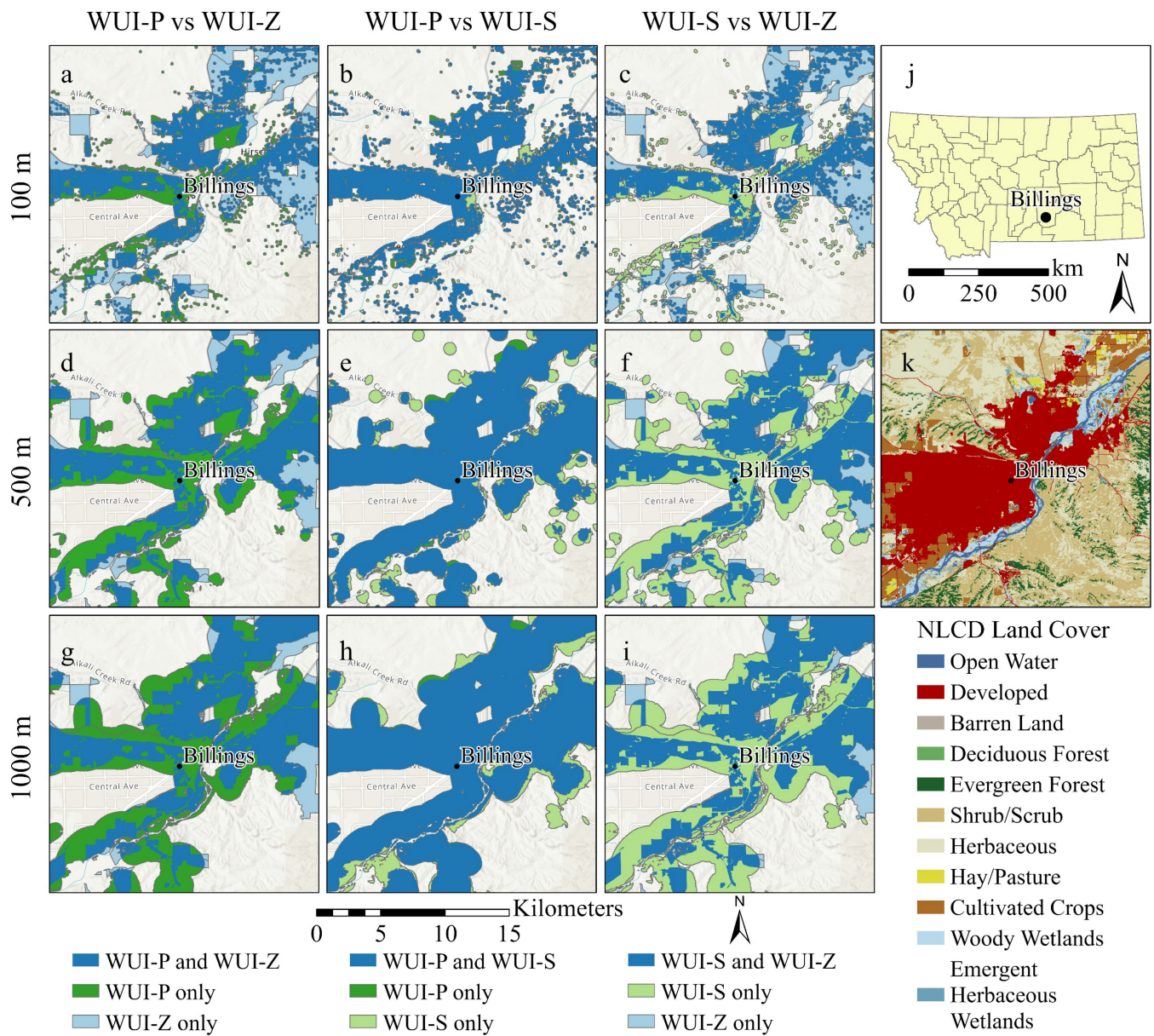
Figure 6. (**a**–**i**) WUI comparison results around Billings, Montana (**j**) at 100 m, 500 m, and 1000 m buffer distances and the land cover map (**k**) in Billings.
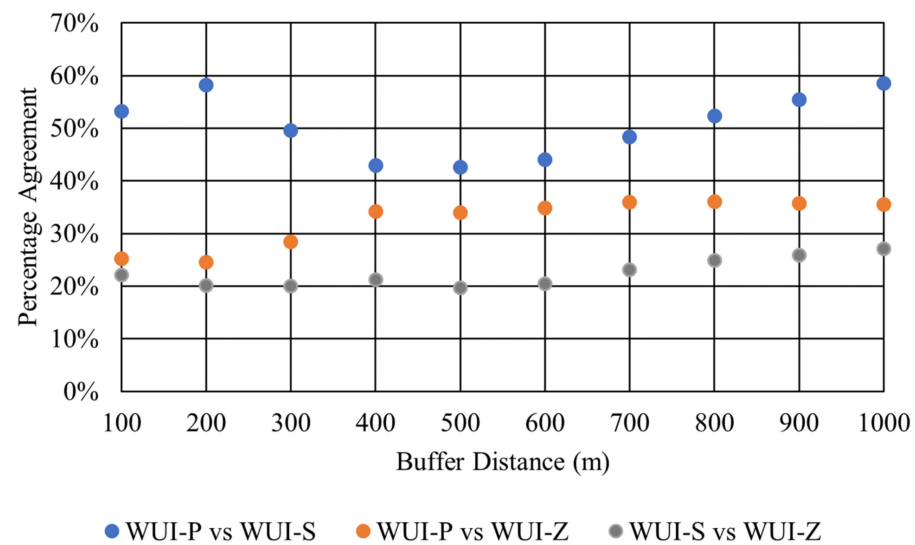
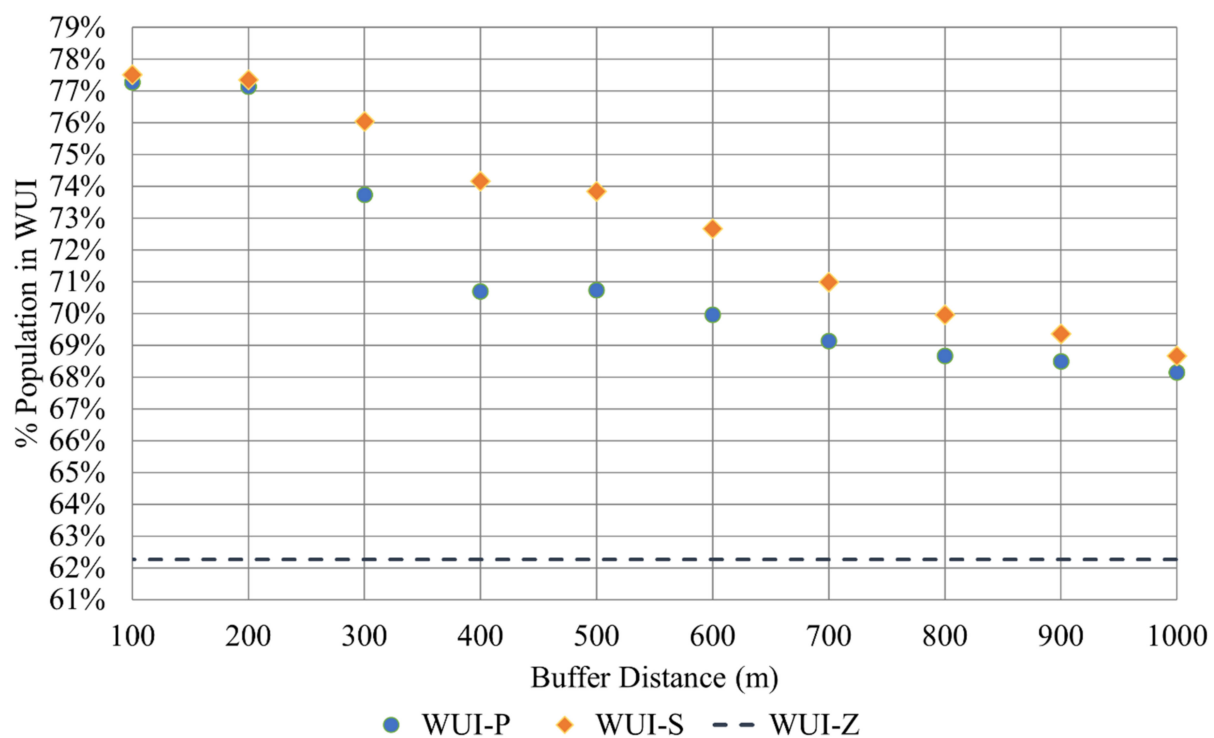**Figure 7.** Percentage agreement between different types of WUI.

Figure 8. Percentage of population within each WUI at different buffer distances.

4.4. The Spatial Patterns of WUI

Table 5 lists the global Moran's I, variance, z-score, and *p*-value for p_a and p_s at each buffer distance for each structure location dataset. In most cases, the results show the presence of spatial clustering, and it is statistically significant with *p*-values below 0.1. In the case of p_a for WUI-P, all buffer distances have global Moran's I values between 0.36 and 0.414 with z-scores between 4.581 and 5.276. The z-scores of p_s for WUI-P differ greatly from those of p_a. The global Moran's I values range from 0.109 to 0.137 and have z-scores that are between 1.588 and 1.881. With these z-scores, the *p*-values are all much less statistically significant. The results for the WUI-P at 100 m, 900 m, and 1000 m buffer distances are not statistically significant, indicating spatial randomness. The results at

all other buffer distances for p_s of the WUI-P are statistically significant. For the WUI-S dataset, the global Moran's I values for p_a in the WUI are all statistically significant ($p = 0.05$ or lower). The global Moran's I values for different buffer distances range from 0.242 to 0.396 and have z-scores between 3.127 and 4.979. The global Moran's I values of p_s range between 0.178 and 0.395 with z-scores ranging between 2.436 and 4.895. Nearly all data points for p_s of the WUI-S have *p*-values below 0.01 except the 100 m buffer data point, which is just above 0.01. Overall, both WUI-S and WUI-P show some level of clustering. Even with p_s of the WUI-P showing less statistical significance than the other data points and variables, it was safe to proceed to perform local Moran's I analysis.

Table 5. Global Moran's I calculation results with variance, z-score, and *p*-value.

WUI Type	Buffer Distance (m)	Area (p_a)				Structures (p_s)			
		Moran's I	Variance	z-Score	*p*-Value	Moran's I	Variance	z-Score	*p*-Value
WUI-P	100	0.360	0.00683	4.581	0.000005	0.109	0.00630	1.602	0.109204
	200	0.374	0.00691	4.722	0.000002	0.115	0.00630	1.675	0.093882
	300	0.379	0.00677	4.833	0.000001	0.126	0.00649	1.785	0.074324
	400	0.393	0.00668	5.027	0.000000	0.124	0.00674	1.733	0.083176
	500	0.411	0.00671	5.243	0.000000	0.137	0.00677	1.880	0.060071
	600	0.414	0.00670	5.276	0.000000	0.136	0.00675	1.881	0.059932
	700	0.408	0.00668	5.213	0.000000	0.126	0.00674	1.753	0.079595
	800	0.405	0.00667	5.182	0.000000	0.120	0.00671	1.691	0.090899
	900	0.403	0.00666	5.161	0.000000	0.116	0.00670	1.642	0.100559
	1000	0.397	0.00665	5.094	0.000000	0.112	0.00669	1.588	0.112349
WUI-S	100	0.273	0.00685	3.516	0.004380	0.178	0.00650	2.436	0.014866
	200	0.288	0.00696	3.669	0.000244	0.196	0.00650	2.655	0.007931
	300	0.265	0.00695	3.392	0.000693	0.200	0.00643	2.715	0.006632
	400	0.242	0.00693	3.127	0.001769	0.207	0.00648	2.798	0.005140
	500	0.243	0.00695	3.128	0.001760	0.222	0.00654	2.967	0.003006
	600	0.277	0.00695	3.540	0.000401	0.283	0.00676	3.665	0.000247
	700	0.332	0.00694	4.198	0.000027	0.342	0.00698	4.312	0.000016
	800	0.370	0.00694	4.661	0.000003	0.386	0.00708	4.802	0.000002
	900	0.386	0.00694	4.857	0.000001	0.391	0.00710	4.860	0.000001
	1000	0.396	0.00693	4.979	0.000001	0.395	0.00711	4.895	0.000001

The local Moran's I analysis generated twenty sets of results for each point dataset: ten for p_a and ten for p_s. Figure 9 shows the results at 100 m, 500 m, and 1000 m buffer distances. These were chosen as examples to show how the clusters differ at small, medium, and large buffer distances. The global Moran's I values for p_s of the WUI-P at the 100 m and 1000 m buffer distances are not statistically significant ($p > 0.1$). In the resulting maps, the dark blue areas represent the low–low (LL) clusters where the values of the percentage of WUI in the county and its surrounding neighbors are lower than average; and the dark red represent the high–high (HH) clusters where the values are higher than average for the county and its neighbors. The counties with lighter colors represent spatial outliers, which have low values (light blue) or high values (light red) surrounded by neighboring counties with dissimilar values and are considered statistically significant. For p_a, the differences at each buffer distance are subtle, even between the two datasets. In each map for p_a, the LL clusters are predominantly in the east and the HH clusters in the west. Of the counties with larger populations in Montana, only Missoula County is classified as HH in all p_a maps with Flathead classified as HH in others. However, some lower population counties in the western portion of the state are also labeled as HH clusters at various buffer levels, which may indicate that population is not an important factor. A possible factor that could be driving the HH clusters is the mountainous terrain in western Montana along with the LL clusters that occur in the eastern plains. However, several of the LL cluster counties are those with small populations. In contrast to p_a, p_s varies much more as the buffer distance changes. With the smaller buffer distances, more HH clusters appear in the east with very

few clusters (HH and LL) or outliers (HL and LH) in the west. This could be due to more individual structures being counted as within the WUI as the 100 m buffer surrounding a single structure will define that area as WUI due to the structure density threshold being met. As the buffer distance increases, fewer individual structure/address points will be included in the WUI.

4.5. A Web GIS Application for Mapping the WUI

The developed web GIS application can be accessed at https://tinyurl.com/2p8rajju (accessed on 16 July 2022). The GUI for the web GIS is shown in Figure 10. A simple GUI was used to ensure intuitive usability, giving the user the ability to compare different WUI maps. The web GIS application includes three linked maps that can show the same location when a user navigates the map via the zoom or pan tool. All three maps have a search icon that can be used to find any location. The home icon will return the view to the default view of the entire state. For the WUI-P and WUI-S maps, a select layer widget is available that allows the user to show or hide the available layers that include the WUI layers for all buffer distances as well as the respective structure point data layer that was used to generate the WUI. The lower three panels contain further information related to the research and guidelines on how to use the web GIS application.
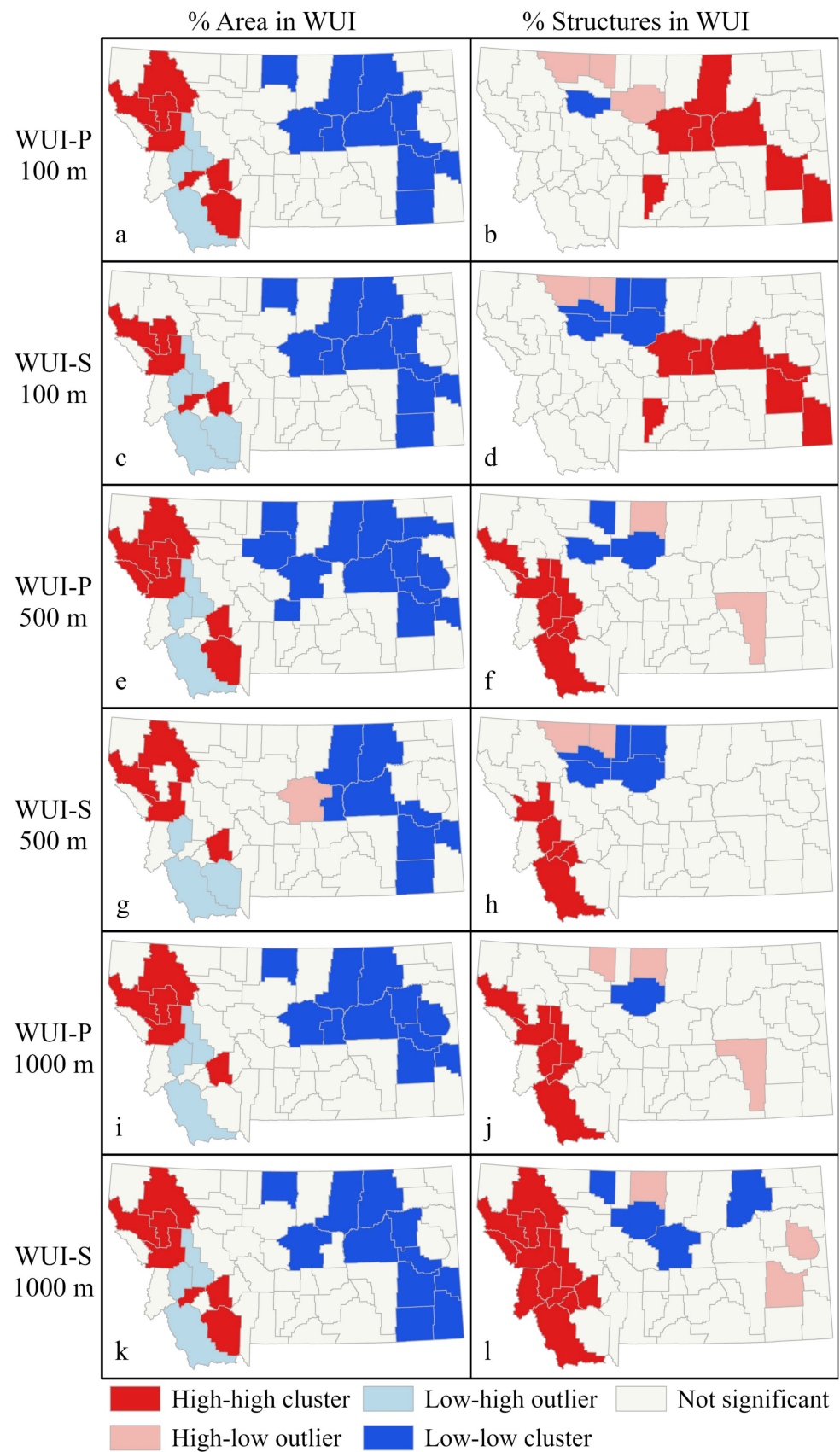
% Area in WUI   % Structures in WUI

Figure 9. The local Moran's I results for WUI-P and WUI-S at 100 m (**a–d**), 500 m (**e–h**), and 1000 m (**i–l**) buffer distances.
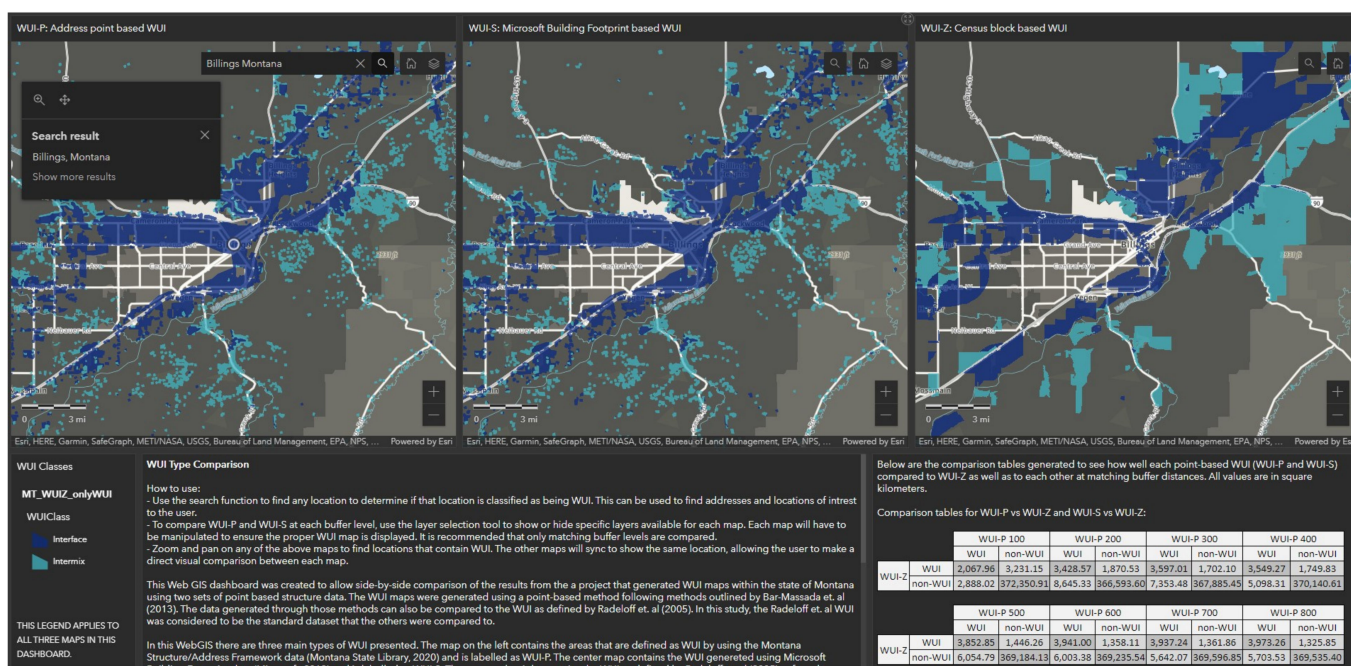
Figure 10. The WUI in Billings, Montana in the web GIS application.

5. Discussion

The first goal of this study was to use two different structure location datasets to generate WUI maps with multiple buffer distances in Montana. The generated WUI maps show how the buffer distance affects the total area of interface and intermix WUI. In the case of the total area, the patterns of WUI-P and WUI-S related to buffer distance presented in this study are similar to those shown in a previous study done by Bar-Massada et al. [28] in some ways but differ in relation to at which buffer distance the highest area of WUI occurs. We found that the intermix WUI has a greater total area as compared to interface WUI in our study, which aligns with the findings in the previous study [28]. Another similarity between the two studies is that the interface WUI area in WUI-P peaks at the same buffer distance of 200 m. However, the intermix WUI in our study peaks at 200 m, while the intermix WUI in all study areas in the previous study conducted by Bar-Massada et al. [28] peaks at larger buffer distances. This difference could be due to the larger area of our study site. As for the behavior of WUI-S in this study, the peak area for both intermix and interface WUI occurs at the 500 m buffer and then decreases. Similar to the previous study conducted by Bar-Massada et al. [28], the smallest area occurs at the 100 m buffer distance. The trend that appears when examining the number of structures within the WUI as the buffer distance changes is distinct from the trend in WUI area. The number of structures that fall within WUI-P and WUI-Z is the greatest at the smallest buffer and decreases as the buffer size increases. This trend is consistent with the results found in a previous study conducted by Bar-Massada et al. [28] and a more recent study done by Carlson et al. [39]. We employed the buffer distances used by Bar-Massada et al. in a previous study [28] to compare the two structure location datasets in WUI mapping. Although buffer distance will affect the derived WUI, little research has been conducted to examine the ideal buffer distance for different types of applications in WUI management. Future research needs to be conducted to further identify the ideal buffer distance for different WUI applications. For example, we can use historical house loss data and the WUI generated with different buffer distances to determine the ideal buffer distance for generating WUI maps that can be used for relevant applications related to house loss.

The results of the map comparison analysis in this study are similar to the findings in the previous study done by Bar-Massada et al. [28] with regard to WUI-P. The percentage agreement between WUI-P and WUI-Z for Montana is similar to the percent-

age agreement within the Grand County, Colorado in the previous study conducted by Bar-Massada et al. [28], which could be related to the similarities in topography, as both study areas contain mountainous and flat terrains. The percentage agreement between WUI-S and WUI-Z is lower than that in the previous study [28]. The lower level of agreement between WUI-S and WUI-Z could be due to the larger number of structures included in the MBF dataset as compared to the Montana address/structure framework dataset. The increased number of structures would likely have the greatest impact on the rural areas where outbuildings are included in the MBF dataset but are not in the address point dataset. It could be possible to refine the MBF data to reduce the number of structures and include only the structures that could be residential. One potential way to accomplish this could be to classify each structure in the MBF dataset by performing a spatial join using the OpenStreetMap (OSM) land use polygon data to determine which structures could be classified as residential. Then we can eliminate the non-residential structures and those structures that are identified as residential but are too small (e.g., sheds or other outbuildings) or too large (e.g., commercial structures or schools) [37]. The abovementioned procedure could increase the agreement between the WUI-S and WUI-Z as the WUI-Z dataset structure density is based on housing units and does not consider non-residential structures. As the Montana address framework dataset does not include a standardized classification system for all addresses, we can use the OSM land use dataset to determine if an address point is in a residential polygon and remove all non-residential address points. This can increase the agreement between WUI-P and WUI-Z. Note that OSM data can be inconsistent in terms of data quality because OSM is a crowdsourcing project [53]. Thus, more research on the data quality of OSM data should be conducted if we use OSM data to improve WUI mapping. Additionally, the population estimation procedure in this study evenly distributes the population over all structure points within a block group. Thus, trimming each structure point dataset can also improve the accuracy of the WUI population estimates. It should be noted that the necessity of the data trimming process depends on the intent and purpose of the WUI to be generated.

The spatial analysis shows distinct patterns between p_a and p_s at smaller buffer distances, and the patterns differ less at larger buffer distances. The spatial patterns for the two variables at each buffer distance do not differ significantly between WUI-P and WUI-S. However, the difference between p_a and p_s within the WUI is apparent. For p_a, the LL clusters are in the eastern portion of Montana, while HH clusters are concentrated in the western part of the state. These patterns are possibly linked to the population distribution within the state. These patterns remain mostly constant as the buffer distance increases. In contrast, the cluster patterns shown for p_s are sensitive to the increase in buffer distance. At smaller buffer distances the HH clusters are predominantly in the east, likely due to the inclusion of individual structures at those buffer distances. As the buffer distance increases, fewer HH clusters are identified in the east with more appearing in the western portion of the state. The greater shift of the clusters could be related to a higher sensitivity of p_s due to the change in the number of structures required to meet the structure density threshold as buffer distance increases. More research related to the spatial patterns of WUI could help explain the sensitivity of the cluster patterns.

Lastly, the WUI maps that have been compared in this study may beg the question of which dataset or buffer distance best represents the location of the WUI. This is a challenging question as the selection of method or dataset depends on the purpose of the WUI maps and the availability of relevant data in a study area [7,40]. For example, the homeowners in Montana may find the WUI-S generated using the MBF with a 100 m buffer distance to be most useful as the defensible space distance recommended by Montana DNRC [54] is less than 100 m and a single structure will meet the density threshold for WUI [39]. The WUI-S (100 m buffer distance) will allow homeowners to easily identify any structure on their property that may be at risk to wildfire damage. The best buffer distance for community planners and wildfire managers is 500 m as the number of structures required to meet the

structure density threshold is closest to the structure density in the WUI definition widely used for wildfire management or community planning purposes [39].

6. Conclusions

As wildfire risk in populated areas continues to grow, it is essential to have tools available to aid wildfire-related decision-making. By mapping the WUI, higher-risk areas can be clearly identified. Understanding what areas are classified as WUI is critical to keeping people and property safe and reducing wildfire risk through wildfire mitigation, fuel reduction, public education, and government regulation at various levels. The contributions of this study are as follows. First, this study provides a systematical comparison of address point data and the MBF dataset in WUI mapping, which can help researchers and practitioners develop a better understanding of these two types of structure location data and their pros and cons in WUI mapping. Our results demonstrate that the MBF dataset works well as a basis for calculating WUI in the same manner as the address point dataset. While the area calculated as WUI-S and WUI-P is larger and more precise than that of WUI-Z, there are still some limitations as it is more computationally intensive and may require some additional expertise to derive point-based WUI. Second, our results can help researchers and practitioners develop a better understanding of the parameters used to map the WUI and their impacts on the potential applications of the WUI maps. Lastly, this study also provides a web GIS application that allows different types of users to access the WUI maps for different applications. This can help researchers and practitioners better present and share their WUI maps in different applications. Finally, based on the results of our state-level study, researchers and practitioners can conduct further research to assess the variations in the methods and parameters used to map the WUI and the applicability of the methods at the national scale.

Institutional Review Board Statement: Not applicable.

Informed Consent Statement: Not applicable.

Data Availability Statement: The Microsoft Building Footprint Dataset of Montana can be downloaded at https://usbuildingdata.blob.core.windows.net/usbuildings-v2/Montana.geojson.zip (accessed on 24 March 2021); The Montana Structure and Address Framework Dataset can be downloaded at https://ftpgeoinfo.msl.mt.gov/Data/Spatial/MSDI/AddressStructures/StructuresFramework_shp.zip (accessed on 24 March 2021); and the 2016 NLCD can be downloaded at https://www.mrlc.gov/data/nlcd-2016-land-cover-conus (accessed on 24 March 2021).

Conflicts of Interest: The authors declare no conflict of interest.

Appendix A

Table A1. The area shared between different types of WUI (unit: km^2).

	WUI-Z	WUI-P 100	WUI-P 200	WUI-P 300	WUI-P 400	WUI-P 500	WUI-P 600	WUI-P 700	WUI-P 800	WUI-P 900	WUI-P 1000
WUI-Z	5299.1	2068.0	3428.6	3597.0	3549.3	3852.8	3941.0	3937.2	3973.3	4026.5	4030.2
WUI-S 100	2075.9	3870.8	5025.7	4100.6	3392.2	3426.6	3308.6	3161.4	3089.1	3063.4	3009.6
WUI-S 200	3405.0	4402.2	9970.3	8069.6	6287.7	6490.7	6222.8	5858.1	5699.2	5653.8	5533.9
WUI-S 300	3780.7	4283.7	9677.9	9375.1	7323.3	7630.1	7301.9	6850.3	6659.8	6606.7	6457.7
WUI-S 400	3859.2	3983.2	8668.9	8783.4	7628.4	8048.8	7701.8	7226.2	7019.5	6952.6	6789.4
WUI-S 500	4132.8	4009.0	8768.5	8926.3	7827.9	8898.8	8663.7	8131.2	7915.5	7859.8	7673.0
WUI-S 600	4231.0	3865.0	8288.9	8587.1	7712.7	8874.5	9036.7	8584.8	8395.5	8353.9	8158.6
WUI-S 700	4241.3	3648.9	7588.2	8008.9	7428.1	8594.9	8887.9	8744.3	8656.7	8647.4	8454.4
WUI-S 800	4274.2	3526.0	7203.4	7652.5	7226.4	8389.8	8745.1	8708.5	8864.0	8959.9	8797.1
WUI-S 900	4314.0	3460.5	7003.6	7447.0	7093.6	8253.5	8646.8	8655.4	8879.9	9181.0	9115.4
WUI-S 1000	4316.6	3371.8	6746.0	7190.7	6915.8	8049.6	8464.8	8517.8	8777.2	9140.2	9244.9

Table A2. Percent agreement between different types of WUI.

	WUI-Z	WUI-S 100	WUI-S 200	WUI-S 300	WUI-S 400	WUI-S 500	WUI-S 600	WUI-S 700	WUI-S 800	WUI-S 900	WUI-S 1000
WUI-Z	100.0%	22.1%	20.1%	20.0%	21.2%	19.6%	20.4%	23.1%	24.9%	25.8%	27.1%
WUI-P 100	25.3%	53.3%	28.3%	23.8%	22.5%	19.3%	18.6%	19.6%	20.1%	20.1%	20.4%
WUI-P 200	24.6%	38.0%	58.2%	49.0%	43.0%	37.8%	35.4%	34.9%	34.3%	33.7%	33.3%
WUI-P 300	28.4%	31.5%	45.1%	49.5%	46.5%	40.8%	39.0%	39.6%	39.4%	38.7%	38.4%
WUI-P 400	34.1%	29.7%	36.2%	39.2%	43.0%	37.8%	37.5%	40.2%	41.2%	41.1%	41.5%
WUI-P 500	33.9%	27.1%	35.2%	38.9%	43.3%	42.6%	42.9%	46.2%	47.6%	47.5%	47.9%
WUI-P 600	34.9%	25.8%	33.2%	36.5%	40.6%	40.9%	44.0%	48.5%	50.5%	50.8%	51.5%
WUI-P 700	36.0%	25.1%	31.3%	34.1%	37.9%	38.1%	41.6%	48.3%	51.3%	52.0%	53.2%
WUI-P 800	36.1%	24.2%	30.0%	32.7%	36.2%	36.6%	40.1%	47.3%	52.4%	53.8%	55.4%
WUI-P 900	35.7%	23.3%	29.2%	31.8%	35.1%	35.7%	39.2%	46.4%	52.2%	55.5%	57.8%
WUI-P 1000	35.5%	22.7%	28.3%	30.8%	33.9%	34.4%	37.8%	44.7%	50.5%	54.6%	58.6%

References

1. Radeloff, V.C.; Helmers, D.P.; Kramer, H.A.; Mockrin, M.H.; Alexandre, P.M.; Bar-Massada, A.; Butsic, V.; Hawbaker, T.J.; Martinuzzi, S.; Syphard, A.D.; et al. Rapid growth of the US wildland-urban interface raises wildfire risk. *Proc. Natl. Acad. Sci. USA* **2018**, *115*, 3314–3319. [CrossRef]
2. Theobald, D.M.; Romme, W.H. Expansion of the US wildland–urban interface. *Landsc. Urban Plan.* **2007**, *83*, 340–354. [CrossRef]
3. Burke, M.; Driscoll, A.; Heft-Neal, S.; Xue, J.; Burney, J.; Wara, M. The changing risk and burden of wildfire in the United States. *Proc. Natl. Acad. Sci. USA* **2021**, *118*, e2011048118. [CrossRef] [PubMed]
4. Glickman, D.; Babbitt, B. Urban wildland interface communities within the vicinity of federal lands that are at high risk from wildfire. *Fed. Regist.* **2001**, *66*, 751–777.
5. Stewart, S.I.; Radeloff, V.C.; Hammer, R.B.; Hawbaker, T.J. Defining the Wildland-Urban Interface. *J. For.* **2007**, *105*, 201–207.
6. Radeloff, V.C.; Hammer, R.B.; Stewart, S.I.; Fried, J.S.; Holcomb, S.S.; McKeefry, J.F. The wildland-urban interface in the United States. *Ecol. Appl.* **2005**, *15*, 799–805. [CrossRef]
7. Stewart, S.I.; Wilmer, B.; Hammer, R.B.; Aplet, G.H.; Hawbaker, T.J.; Miller, C.; Radeloff, V.C. Wildland-Urban Interface Maps Vary with Purpose and Context. *J. For.* **2009**, *107*, 78–83.
8. Johnston, L.M.; Flannigan, M.D. Mapping Canadian wildland fire interface areas. *Int. J. Wildland Fire* **2018**, *27*, 1–14. [CrossRef]
9. Balch, J.K.; Bradley, B.A.; Abatzoglou, J.T.; Nagy, R.C.; Fusco, E.J.; Mahood, A.L. Human-started wildfires expand the fire niche across the United States. *Proc. Natl. Acad. Sci. USA* **2017**, *114*, 2946–2951. [CrossRef]
10. Parisien, M.-A.; Miller, C.; Parks, S.A.; DeLancey, E.R.; Robinne, F.-N.; Flannigan, M.D. The spatially varying influence of humans on fire probability in North America. *Environ. Res. Lett.* **2016**, *11*, 075005. [CrossRef]
11. Dennison, P.E.; Brewer, S.C.; Arnold, J.D.; Moritz, M.A. Large wildfire trends in the western United States, 1984–2011. *Geophys. Res. Lett.* **2014**, *41*, 2928–2933. [CrossRef]
12. Holden, Z.A.; Swanson, A.; Luce Charles, H.; Jolly, W.M.; Maneta, M.; Oyler Jared, W.; Warren Dyer, A.; Parsons, R.; Affleck, D. Decreasing fire season precipitation increased recent western US forest wildfire activity. *Proc. Natl. Acad. Sci. USA* **2018**, *115*, E8349–E8357. [PubMed]
13. Abatzoglou, J.T.; Williams, A.P. Impact of anthropogenic climate change on wildfire across western US forests. *Proc. Natl. Acad. Sci. USA* **2016**, *113*, 11770–11775. [CrossRef] [PubMed]
14. Abatzoglou, J.T.; Juang, C.S.; Williams, A.P.; Kolden, C.A.; Westerling, A.L. Increasing Synchronous Fire Danger in Forests of the Western United States. *Geophys. Res. Lett.* **2021**, *48*, e2020GL091377.
15. Miller, C.; Ager, A.A. A review of recent advances in risk analysis for wildfire management. *Int. J. Wildland Fire* **2013**, *22*, 1–14.
16. Haynes, K.; Short, K.; Xanthopoulos, G.; Viegas, D.; Ribeiro, L.M.; Blanchi, R. Wildfires and WUI fire fatalities. In *Encyclopedia of Wildfires and Wildland-Urban Interface (WUI) Fires*; Manzello, S.L., Ed.; Springer: Cham, Switzerland, 2020; p. 16.
17. Nagy, R.C.; Fusco, E.; Bradley, B.; Abatzoglou, J.T.; Balch, J. Human-Related Ignitions Increase the Number of Large Wildfires across U.S. Ecoregions. *Fire* **2018**, *1*, 4. [CrossRef]
18. Alexandre, P.M.; Stewart, S.I.; Keuler, N.S.; Clayton, M.K.; Mockrin, M.H.; Bar-Massada, A.; Syphard, A.D.; Radeloff, V.C. Factors related to building loss due to wildfires in the conterminous United States. *Ecol. Appl.* **2016**, *26*, 2323–2338. [PubMed]
19. Alexandre, P.M.; Stewart, S.I.; Mockrin, M.H.; Keuler, N.S.; Syphard, A.D.; Bar-Massada, A.; Clayton, M.K.; Radeloff, V.C. The relative impacts of vegetation, topography and spatial arrangement on building loss to wildfires in case studies of California and Colorado. *Landsc. Ecol.* **2016**, *31*, 415–430.
20. Syphard, A.D.; Keeley, J.E. Factors associated with structure loss in the 2013–2018 California wildfires. *Fire* **2019**, *2*, 49. [CrossRef]
21. Syphard, A.D.; Keeley, J.E.; Massada, A.B.; Brennan, T.J.; Radeloff, V.C. Housing arrangement and location determine the likelihood of housing loss due to wildfire. *PLoS ONE* **2012**, *7*, e33954.
22. Ager, A.A.; Palaiologou, P.; Evers, C.R.; Day, M.A.; Ringo, C.; Short, K. Wildfire exposure to the wildland urban interface in the western US. *Appl. Geogr.* **2019**, *111*, 102059.
23. Caggiano, M.D.; Hawbaker, T.J.; Gannon, B.M.; Hoffman, C.M. Building Loss in WUI Disasters: Evaluating the Core Components of the Wildland–Urban Interface Definition. *Fire* **2020**, *3*, 73.
24. Kramer, H.A.; Mockrin, M.H.; Alexandre, P.M.; Radeloff, V.C. High wildfire damage in interface communities in California. *Int. J. Wildland Fire* **2019**, *28*, 641–650.
25. Kramer, H.A.; Mockrin, M.H.; Alexandre, P.M.; Stewart, S.I.; Radeloff, V.C. Where wildfires destroy buildings in the US relative to the wildland–urban interface and national fire outreach programs. *Int. J. Wildland Fire* **2018**, *27*, 329–341.
26. Haight, R.G.; Cleland, D.T.; Hammer, R.B.; Radeloff, V.C.; Rupp, T.S. Assessing fire risk in the wildland-urban interface. *J. For.* **2004**, *102*, 41–48.
27. Moritz, M.A.; Batllori, E.; Bradstock, R.A.; Gill, A.M.; Handmer, J.; Hessburg, P.F.; Leonard, J.; McCaffrey, S.; Odion, D.C.; Schoennagel, T.; et al. Learning to coexist with wildfire. *Nature* **2014**, *515*, 58–66.
28. Bar-Massada, A.; Stewart, S.I.; Hammer, R.B.; Mockrin, M.H.; Radeloff, V.C. Using structure locations as a basis for mapping the wildland urban interface. *J. Environ. Manag.* **2013**, *128*, 540–547.
29. Platt, R.V. The wildland–urban interface: Evaluating the definition effect. *J. For.* **2010**, *108*, 9–15.
30. Argañaraz, J.P.; Radeloff, V.C.; Bar-Massada, A.; Gavier-Pizarro, G.I.; Scavuzzo, C.M.; Bellis, L.M. Assessing wildfire exposure in the Wildland-Urban Interface area of the mountains of central Argentina. *J. Environ. Manag.* **2017**, *196*, 499–510.

31. Conedera, M.; Tonini, M.; Oleggini, L.; Vega Orozco, C.; Leuenberger, M.; Pezzatti, G.B. Geospatial approach for defining the Wildland-Urban Interface in the Alpine environment. *Comput. Environ. Urban Syst.* **2015**, *52*, 10–20.
32. Lampin-Maillet, C.; Jappiot, M.; Long, M.; Bouillon, C.; Morge, D.; Ferrier, J.-P. Mapping wildland-urban interfaces at large scales integrating housing density and vegetation aggregation for fire prevention in the South of France. *J. Environ. Manag.* **2010**, *91*, 732–741.
33. Miranda, A.; Carrasco, J.; González, M.; Pais, C.; Lara, A.; Altamirano, A.; Weintraub, A.; Syphard, A.D. Evidence-based mapping of the wildland-urban interface to better identify human communities threatened by wildfires. *Environ. Res. Lett.* **2020**, *15*, 094069.
34. Calkin, D.E.; Rieck, J.D.; Hyde, K.D.; Kaiden, J.D. Built structure identification in wildland fire decision support. *Int. J. Wildland Fire* **2011**, *20*, 78–90.
35. Li, D.; Cova, T.J.; Dennison, P.E.; Wan, N.; Nguyen, Q.C.; Siebeneck, L.K. Why do we need a national address point database to improve wildfire public safety in the U.S.? *Int. J. Disaster Risk Reduct.* **2019**, *39*, 101237.
36. Microsoft. US Building Footprints. Available online: https://github.com/microsoft/USBuildingFootprints (accessed on 23 March 2021).
37. Huang, X.; Wang, C.; Li, Z.; Ning, H. A 100 m population grid in the CONUS by disaggregating census data with open-source microsoft building footprints. *Big Earth Data* **2021**, *5*, 1–22.
38. Huang, X.; Wang, C. Estimates of exposure to the 100-year floods in the conterminous United States using national building footprints. *Int. J. Disaster Risk Reduct.* **2020**, *50*, 101731.
39. Carlson, A.R.; Helmers, D.P.; Hawbaker, T.J.; Mockrin, M.H.; Radeloff, V.C. The wildland-urban interface in the United States based on 125 million building locations. *Ecol. Appl.* **2022**, *32*, e2597.
40. Bar-Massada, A. A Comparative Analysis of Two Major Approaches for Mapping the Wildland-Urban Interface: A Case Study in California. *Land* **2021**, *10*, 679.
41. Li, S.; Dao, V.; Kumar, M.; Nguyen, P.; Banerjee, T. Mapping the wildland-urban interface in California using remote sensing data. *Sci. Rep.* **2022**, *12*, 5789.
42. Whitlock, C.; Cross, W.; Maxwell, B.; Silverman, N.; Wade, A. *Montana Climate Assessment*; Montana State University: Bozeman, MT, USA, 2017; p. 18.
43. Adams, A.; Byron, R.; Maxwell, B.; Higgins, S.; Eggers, M.; Byron, L.; Whitlock, C. *Climate Change and Human Health in Montana: A Special Report of the Montana Climate Assessment*; Montana State University: Bozeman, MT, USA, 2021; p. 14.
44. Radeloff, V.C.; Mockrin, M.H.; Helmers, D.P.; Mapping Change in the Wildland Urban Interface (WUI) 1990–2010. State Summary Statistics June 2018. Available online: http://silvis.forest.wisc.edu/GeoData/WUI_cp12/WUI_change_1990_2010_State_Stats_Report.pdf (accessed on 4 April 2021).
45. U.S. Census Bureau. Available online: https://www.census.gov/quickfacts/MT (accessed on 15 July 2022).
46. Tapp, A.F. Areal interpolation and dasymetric mapping methods using local ancillary data sources. *Cartogr. Geogr. Inf. Sci.* **2010**, *37*, 215–228.
47. Zandbergen, P.A. Dasymetric mapping using high resolution address point datasets. *Trans. GIS* **2011**, *15*, 5–27.
48. Anselin, L. Local indicators of spatial association—LISA. *Geogr. Anal.* **1995**, *27*, 93–115.
49. Bolstad, P. *GIS Fundamentals: A First Text on Geographic Information Systems*, 6th ed.; Eider Press: White Bear Lake, MN, USA, 2019.
50. Harris, R. *Quantitative Geography: The Basics*; Sage: London, UK, 2016.
51. Environmental Systems Research Institute. ArcGIS Online. Available online: https://www.arcgis.com (accessed on 23 March 2021).
52. Fu, P.; Sun, J. *Web GIS: Principles and Applications*; ESRI Press: Redlands, CA, USA, 2011.
53. Sehra, S.S.; Singh, J.; Rai, H.S. A Systematic Study of OpenStreetMap Data Quality Assessment. In Proceedings of the 2014 11th International Conference on Information Technology: New Generations, Las Vegas, NV, USA, 7–9 April 2014; pp. 377–381.
54. Montana DNRC. Guidelines for Development within the Wildland-Urban Interface. 2009. Available online: http://dnrc.mt.gov/divisions/forestry/docs/fire-and-aviation/prevention/guidelinesfinal.pdf (accessed on 24 March 2021).